# Raman spectroscopy investigation of biochemical changes in tumour spheroids with ageing and after treatment with staurosporine

*Lauren E. Jamieson*[1], *David J. Harrison*[2], *Colin J. Campbell*[1,*]

*Corresponding Author: E-mail: colin.campbell.ed.ac.uk

[1] School of Chemistry, University of Edinburgh, Joseph Black Building, David Brewster Road, Edinburgh EH9 3FJ, UK
[2] School of Medicine, University of St Andrews, North Haugh, St Andrews KY16 9TF, UK

Keywords: multicellular tumour spheroids, Raman, cancer, drug screening

There has been increasing use of *in vitro* cell culture models that more realistically replicate the three dimensional (3D) environment found *in vivo.* Multicellular tumour spheroids (MTS) using cell lines or patient-derived organoids have become an important *in vitro* drug development tool, where cells are grown in a 3D 'sphere' that exhibits many of the characteristics found *in vivo*. Significantly, MTS develop gradients in nutrients and oxygen, commonly found in tumours, that contribute to therapy resistance. While MTS show promise as a more realistic *in vitro* culture model, there is a massive need to improve imaging technologies for assessing biochemical characteristics and drug response in such models to maximize their translation into useful applications such as high throughput screening (HTS). In this study we investigate the potential for Raman spectroscopy to unveil biochemical information in MTS and have investigated how spheroid age influences drug response, shedding light on increased therapy resistance in developing tumours. The wealth of molecular level information delivered by Raman spectroscopy in a noninvasive manner, could aid translation of these 3D models into HTS applications.



This article has been accepted for publication and undergone full peer review but has not been through the copyediting, typesetting, pagination and proofreading process, which may lead to differences between this version and the Version of Record. Please cite this article as doi: 10.1002/jbio.2201800201

## 1. Introduction

Drug and therapy resistance is a major issue in cancer therapeutics, with drug efficacy often failing to translate into the *in vivo* environment from *in vitro* studies.[1, 2] One of the pitfalls of conventional *in vitro* models is that the cells exist in a two dimensional environment; growing on a flat surface that does not accurately reflect the three dimensional architecture of the body.[3, 4] Therefore, studies of both underlying biochemistry and drug efficacy screening can often be misleading due to the simplified environment. Use of *ex vivo* and *in vivo* models can resolve many of these issues, however, access to such samples is limited and requires extensive ethical consideration before these can be used, particularly for *in vivo* studies. Therefore, while they provide a more realistic environment, it is difficult to meet the high throughput demands that *in vitro* models can provide.[5] In recent years, attention has turned to 3D *in vitro* models that involve growing cells in a three dimensional environment that more closely resembles that found in the body.[6] Cells can be mixed with and grown in both natural and synthetic scaffolds such as collagen[7] and peptide hydrogels[8] respectively. One popular 3D culture method is the formation of multicellular tumour spheroids (MTS). In particular, these mimic the physiological characteristics of cancer tumours by developing gradients in characteristics such as oxygen concentration, nutrient concentration and pH, similar to those found as a cancer tumour grows in the body.[4, 9] As a tumour grows, central regions become cut-off from the well-organised vasculature of the body that supplies oxygen and nutrients to cells. Despite cancer cells signaling for formation of new blood vessels[10], the vessels tend to be disorganised and leaky, with no pressure differential to encourage flow, therefore failing to meet adequate oxygen and nutrient demands typical of normal cells.[11, 12] Therefore, gradients develop, often leading to the formation of hypoxic core regions in bloodflow (and therefore

oxygen) -deprived regions.[13, 14] This hypoxic characteristic can confer resistance to many therapies.[15, 16] While lack of blood vessels makes vascular drug delivery inefficient[17], radiotherapy is also less effective because it relies on the presence of oxygen to form reactive oxygen species to destroy cancer cells. Therefore, MTS can provide an *in vitro* tumor model that can more accurately reflect *in vivo* cancer physiology and responses to therapy.

While these 3D *in vitro* models address many of the biological problems associated with traditional 2D *in vitro* culture, there are limitations with regards to tools for their analysis.[4, 18] For example, techniques such as Western blot, polymerase chain reaction and electrophoresis allow detailed analysis of overall protein and DNA composition, but are destructive and involve lysing the 3D culture to extract biomolecules.[19,20] Such spatially insensitive techniques are also time consuming, and new analytical methods are sought after.[21] Biomolecular imaging of intact cells within MTS is limited primarily by the absence of imaging technologies that allow sufficient depth penetration into a 3D structure. More recent advances have seen successful fluorescence imaging of intact MTS using light sheet fluorescence microscopy where the sample is illuminated by a sheet of light through each plane, followed by collection of emitted light perpendicular to this.[22] Using light sheet fluorescence microscopy, photobleaching and photodamage are limited, 3D structures can be more rapidly imaged whilst still alive and MTS can be imaged over their full depth. Fluorescence imaging itself, however, has its own drawbacks - requiring incorporation of a fluorophore that could interfere with native intracellular biochemistry. In addition, each fluorophore only probes one specific biomolecule, and therefore the biochemical information that can be gained in this way is severely limited.

Raman spectroscopy has been used previously for analysis of biological samples *in vitro*, *ex vivo*, and *in vivo*.[23] It allows samples to be probed in a label-free and non-destructive manner,

giving a high level of chemically specific, molecular level detail. To our knowledge, this technique has not previously been used to analyse therapy response in MTS but Raman[24] and surface enhanced Raman spectroscopy[14, 25, 26] have shown promise previously for measuring characteristics of MTS. Its advantageous characteristics have allowed a detailed biochemical analysis to be made without the need for external labels, providing a high level of spatially resolved biomolecular detail relating to drug-resistance in ageing spheroids. While this study uses fixation, paraffin embedding and sectioning of MTS, which is destructive of the live MTS sample, the analysis of the sectioned sample itself using Raman spectroscopy is non-destructive, and each spheroid section can thus be analysed multiple times. There is also no application of external agents to the sample prior to fixation, such as fluorescence or colorimetric stains, which could alter the innate biochemistry of the sample. Ultimately the capabilities of Raman spectroscopy, investigated in this study, can be extended to analysis of intact live samples. Staurosporine is a protein kinase inhibitor and potent pro-apoptotic agent, with strong anti-cancer properties, and as such was selected as the therapeutic agent of choice to demonstrate the premise of this work.[27] While MCF7 cells lack caspase-3, a key protein in the apoptotic process, it has been demonstrated that staurosporine still induced lethality to MCF7 cells in 2D culture.[28]

## 2. Materials and Methods

**2.1. Cell culture** MCF7 human breast cancer cells (gifted from Division of Pathology Laboratories, Western General Hospital, Edinburgh) were cultured in Dulbecco's Modified Eagle's Medium (DMEM) supplemented with 1% penicillin/streptomycin (10,000 units/ml) and 10% heat-inactivated fetal bovine serum (FBS). Cells were incubated at 37 °C and 5% $CO_2$ in a humidified incubator.

MTS were prepared using the hanging drop technique.[29] MCF7 cell spheroids have previously been successfully grown using a hanging drop[30] and other methods[31], and the hanging drop technique has been optimised for MCF7 MTS through extensive work in our group.[14, 25, 32] Cells were grown in monolayer culture as normal. Cells were trypsinised, pelleted by centrifugation and resuspended in 0.5 ml of medium. 20 µl drops of cell suspension were pipetted onto the lid of a plastic Petri dish and approximately 5-10 ml of medium was added to the bottom of the dish. The lid containing hanging drops was placed on the Petri dish and MTS were grown in the drops over a period of 6, 12 or 15 days.

**2.2. Staurosporine treatment** Medium was removed from hanging drops and replaced with 20 µl of 10 µM staurosporine (STS) in DMEM, for 1 hour.

**2.3. Spheroid fixation** Medium, either with or without STS, was removed from hanging drops and replaced with 20 µl 4% paraformaldehyde. After approximately 10 minutes, MTS were transferred to an Eppendorf and stored in 4% paraformaldehyde.

**2.4. Paraffin embedding and histology** MTS were processed using standard histology procedures for paraffin embedding and sectioning at the Division of Pathology Laboratories, Western General Hospital, Edinburgh. Spheroids were sectioned (3 µm) onto calcium fluoride windows and dewaxed prior to Raman analysis. Adjacent sections were sectioned onto glass slides and stained with Hematoxylin and Eosin.

**2.5. Raman mapping** Raman spectra were acquired on a Renishaw inVia Raman microscope equipped with a 532 nm Nd:YAG laser giving a maximum power of 500 mW, 1800 l/mm grating, and using a Leica 50×/NA 0.75 N PLAN EPI objective. Full MTS sections were mapped using a step size of 5 µm in x and y, 3 s acquisition time, 50% laser power and a

spectral centre of 1300 $cm^{-1}$. The high resolution section through the Day 15 MTS was mapped using a step size of 1 μm in x and y, 1 s acquisition time, 50% laser power and a spectral centre of 1300 $cm^{-1}$.

**2.6. Raman data processing** Pre-processing of all maps was performed using Renishaw Wire 4.2 software. Cosmic rays were removed using the Width of Features algorithm (width parameter 3, height parameter 15) followed by smoothing using Savitsky-Golay smoothing (smooth window 9, polynomial order 3) and finally baseline subtraction.

For full MTS section maps, spectra were then imported into MATLAB R2016a and processed using custom scripts (available on request). Remaining outlier spectra (due to cosmic rays and/or saturation) were removed using the threshold tool followed by selection of cell regions using the threshold tool, both based on total spectral intensity. Spectra were normalised between 0 and 1. A quality control step was applied to the spectral data set from each condition such that all spectra outwith one standard deviation of the mean were removed. This removed poor quality, noisy and outlier spectra and improved further analysis. For principal component analysis (PCA) the relevant data sets were combined in each case, followed by normalising between 0 and 1, and determination of the first derivative of each spectrum using 13 smoothing points. PCA was then performed on the first derivative spectra and results were plotted. First derivative spectra were used to minimise contributions from non-specific baseline variations to the spectral peak variation derived from biological species. In addition, average spectra were plotted for comparison and scatter plots were generated plotting intensity at 963 $cm^{-1}$ and intensity of 1012 $cm^{-1}$. For the Day 15 MTS map, the impoly function was used to separate central and outer regions of the MTS and comparison was then made between these regions using the same processing steps.

For the high resolution map section, principal component analysis was performed in Renishaw Wire 4.2 software using minimum total variance explained (98%) and spectrum centering and normalisation with mean-centre.

For statistical comparison of intensities at 963 $cm^{-1}$ and 1012 $cm^{-1}$, GraphPad Prism 7.03 was used to perform Mann-Whitney tests on the data.

## 3. Results and Discussion

In this study we explored the potential for Raman spectroscopy to be used for detailed analysis of MTS in order to assess important underlying biochemistry, that could be vital for consideration in cancer therapy. Raman analysis was carried out on fixed and sectioned spheroids where the sections provided a representative radial profile of MTS. Highly resolved Raman maps were obtained, with spatial resolution of 1 µm easily obtainable. The biochemical changes in ageing MTS were investigated in a label free manner using Raman spectroscopy, with MTS grown for 6, 12 and 15 days. Additionally, the apoptosis-inducing drug staurosporine (a protein kinase inhibitor) was used to determine sensitivity to drug as a function of spheroid age.

MTS grown over 6, 12 and 15 days, both untreated and treated for 1 hour with 10 µM staurosporine were analysed using Raman spectroscopy. Raman mapping was performed on spheroid sections, with the aim to gain new insight into biochemistry of MTS using this label free and chemically specific vibrational technique. Following spectral processing, spectra extracted from maps for each condition were compared, and adjacent sections stained with haematoxylin and eosin (H&E) (**Figure 1**) provided a comparison with more routine biochemical analytical methodology. Spheroid shapes varied between conditions, which could partly be attributed to sample to sample variation and potential artefacts from fixation and

sectioning procedures. It is noteworthy however that 6 day old MTS appeared to have more densely packed cells than 12 or 15 day old MTS, in keeping with areas of necrosis that develop in older MTS. The difference in shape before and after STS treatment was also more apparent for 6 day old MTS, and in particular the nuclear staining with hematoxylin appeared to indicate only a small necrotic region in the centre of untreated 6 day old MTS where nuclei were condensed and densely packed, but which became more pronounced in STS-treated MTS of the same age. The 15 day old MTS showed a much larger central necrotic region, indicated by the same nuclear pattern, with a less pronounced change in these characteristic necrotic regions in STS treated 15 day old MTS. While no specific molecular markers were used to distinguish proliferative, hypoxic and necrotic regions of MTS, H&E staining confirmed the establishment of a larger necrotic region in older MTS, and a less pronounced change in morphology both at the spheroid and cell level for older MTS.

### 3.1. Investigating biochemical changes induced by STS treatment on MTS of different ages

Principal component analysis (PCA) was used to compare the spectra between MTS of different ages and treatments (**Figure 2**). PCA is an unsupervised multivariate analysis technique that reduces the dimensionality of multivariate data into principal components (PCs) that sequentially describe the primary sources of variation in a data set such that PC1 explains the largest source of variation, followed by PC2 and so on. For each time point, a plot of PC1 and PC2 revealed a separation between untreated and STS treated MTS. The discriminatory power of PCA to distinguish between untreated and STS treated MTS became less apparent as MTS age increased, with a distinct separation in PC2 for 6 day old MTS (Figure 2a), a less distinct separation in PC2 for 12 day old MTS (Figure 2b) and only a nominal separation in PC1 for 15 day old MTS (Figure 2c). Even in 6 day old MTS there was some overlap between non-treated and STS treated MTS, which is probably a result of

variation in response to drug treatment over the area of the MTS such that central more necrotic regions, while perhaps not as developed as in the older MTS, show minimal response to treatment and thus overlap more with the untreated MTS. In order to reveal the particular spectral signals that resulted in these discriminations, PC loadings for the PCs causing the separations were investigated. For 6 day old MTS, PC2 (Figure 2d) loadings revealed the major sources of variation between STS treated and untreated MTS, with PC2 showing a very predominant contribution from a peak around 1012 $cm^{-1}$. For 12 day old MTS, PC2 loadings (Figure 2e) revealed prominent signals at 1004 $cm^{-1}$, 1295 $cm^{-1}$, 1448 $cm^{-1}$ and 963 $cm^{-1}$ that distinguished untreated from STS treated MTS. Finally, for 15 day old MTS, the PC1 loadings (Figure 2f) suggest major contribution from 1295 $cm^{-1}$, 1004 $cm^{-1}$, 1134 $cm^{-1}$, 1063 $cm^{-1}$, 1439 $cm^{-1}$ and 963 $cm^{-1}$.

While peaks at 1063 $cm^{-1}$ , 1134 $cm^{-1}$ ,1295 $cm^{-1}$ and 1439 $cm^{-1}$ probably arise from paraffin (despite dewaxing, see ESI Figure S1 for spectrum of paraffin), spectral features at 1004 $cm^{-1}$, 1295 $cm^{-1}$, 1448 $cm^{-1}$, 1134 $cm^{-1}$ and 1063 $cm^{-1}$ are common strong assignments found in biological Raman spectra assigned to phenylalanine, $CH_2$ group twisting, $CH_2/CH_3$ group scissoring, C-C stretching and C-C stretching respectively.[33, 34] However, the two peaks at 963 $cm^{-1}$ and 1012 $cm^{-1}$ were identified to be prominent distinguishing signals between untreated and STS treated MTS. In order to compare peaks in this region more closely, average spectra for each MTS were plotted and compared (**Figure 3**). In particular focus was directed towards the region between 900 $cm^{-1}$ and 1100 $cm^{-1}$ containing the 963 $cm^{-1}$ and 1012 $cm^{-1}$ peaks. Additionally, in order to simplify comparison, individual spectra from the maps were plotted as scatter plots of intensity of these two peaks (**Figure 4**). These measures highlight the major sources of important spectral variation between MTS. The appearance of a peak at 1012 $cm^{-1}$ for STS treated compared to untreated 6 day old MTS was a major distinguishing feature, highlighted further by the distribution of points in Figure 4a. In comparison, STS treated

compared to untreated 12 day old MTS was distinguished by a loss of signal at 963 $cm^{-1}$. Finally, for 15 day old MTS, the changes in these peaks were indistinct, with the scatter plot in Figure 4c revealing only a small change in these signals with slightly higher intensity at 1012 $cm^{-1}$ for untreated MTS compared to STS treated MTS.

These observations translate to Raman spectra exhibiting increasingly similar profiles for MTS before and after STS treatment as the MTS age increased. As MTS grow they are known to mimick tumour growth by developing gradients in pH, nutrients and oxygen concentration as central regions move further from the supply of these essential components. Eventually these central regions can become necrotic, with an intermediate region of non-proliferating quiescent cells. Similar to hypoxic tumours becoming increasingly resistant to therapy as they grow, MTS may develop increasing resistance as they age, again mimicking closely the characteristics of cancer *in vivo.* Previous studies have demonstrated a relationship between increased levels of hypoxia and necrosis in MTS as they grow over longer time periods and resistance to chemotherapeutic agents including 5-fluorouracil, cisplatin and staurosporine.[13, 35] Therefore, the observation *via* Raman spectroscopy that MTS became increasingly resistant to STS treatment with age is understandable in terms of the underlying biology of the MTS and supports evidence from previous investigations. This adds to previous research outlining the importance of considering spheroid age, and therefore biochemical characteristics, when using MTS in screening assays to mimic the *in vivo* environment – e.g. Däster *et al.*[13] showed that older MTS with hypoxic and necrotic regions had gene expression profiles closer to those observed *in vivo*.

### 3.2. Investigating biochemical changes as a factor of MTS age in untreated and STS treated MTS

In addition to comparing treated to untreated MTS, all untreated MTS and all STS treated MTS were compared on the basis of their age (**Figure 5**). A PC plot of PC1 and PC2 (Figure 5a) revealed a slight discrimination on PC1 and PC2 with MTS ages for untreated MTS. After STS treatment, discrimination between MTS of different ages became more apparent, suggesting that MTS response to STS varied with age. A plot of PC2 and PC3 revealed a distinct separation between STS treated MTS of different ages (Figure 5b). Analysis of spectra revealed an increase in signal at 963 $cm^{-1}$ with spheroid age (Figure 5c), while for STS treated MTS only 15 day old MTS had a strong signal at 963 $cm^{-1}$, with 6 day old MTS having a distinguishing peak at 1012 $cm^{-1}$ (Figure 5d). Again scatter plots of the signal intensity at 963 $cm^{-1}$ and 1012 $cm^{-1}$ clarified these trends, with slight distinction on the basis of 963 $cm^{-1}$ intensity for untreated MTS (Figure 5e), and clear separation of all three STS treated MTS (Figure 5f).

In terms of molecular changes in the ageing MTS identified using Raman spectroscopy, the peaks observed at 963 $cm^{-1}$ and 1012 $cm^{-1}$ probably originate from cellular DNA. An extensive study into Raman spectroscopy of various DNA bases and changes in response to radiation damage observed changes to peaks in these regions as a result of radiation damage to DNA bases, similar to those observed in this study.[36] A peak at 1012 $cm^{-1}$ is assigned to a furanose vibration and we propose that the appearance of this peaks can be correlated with cellular DNA damage. Ruiz-Chica *et al.*[37] also associated a peak at 1012 $cm^{-1}$ with deoxyribose ring stretching. This peak is not commonly observed in Raman spectra of healthy cells and therefore it is possible that its presence reports on structural changes to cellular DNA, including age and drug induced damage to cellular DNA as a result of apoptosis or necrosis. The peak at 963 $cm^{-1}$ could also be an indicator of DNA damage and suggests a different mode of DNA damage as MTS age. However, this peak also matches that assigned to calcium hydroxyapatite and it is possible that it indicates the formation of microcalcifications as the

MTS age.[38] Analysis of H&E stained sections indicates some inclusions that could be microcalcifications but they present a less clear distinction between MTS of different ages – further work is required to definitively assign this peak.

### 3.3. Investigating zonation dependent intra-MTS biochemical variations

In order to investigate these molecular changes further, the 15 day old MTS, which visually showed distinct zonation indicating a necrotic core (central region) surrounded by outer proliferating cells (outer region), was analysed in detail (Figure 1). Central and outer regions were separated based on visual inspection and compared using the same procedures used for previous analysis between conditions (**Figure 6**). PCA revealed a spectral separation on PC4, which was explained by the two peaks already indicated as the major sources of variation – 1012 $cm^{-1}$ and 963 $cm^{-1}$. Combined with analysis of the average spectra in this region and scatter plots of intensity of these peaks, it was clear that central regions manifested a presence of the peak at 1012 $cm^{-1}$, and while the 963 $cm^{-1}$ peak was present in both regions, it was more predominant in the outer region. Therefore, in addition to distinguishing different MTS, these spectral signatures showed important variation within individual MTS. It is important to relate this back to observations made on the H&E stained MTS sections (Figure 1), where the central region of the 15 day old MTS was most obviously necrotic, with condensed, densely packed nuclear regions, similar in pattern to regions appearing in the STS treated 6 day old MTS. This further supports the association of the peak at 1012 $cm^{-1}$ with DNA and DNA damage. There is also inconclusive staining observed in the outer region of the 15 day old MTS, where darker stained regions not typical in shape to nuclei, could indicate foci of microcalcification.

The only other section which had a visibly distinguishable necrotic region was the 6 day old MTS. In this case there was no obvious separation between central and outer regions using

PCA (Figure S2), however this could be expected as these much younger MTS were unlikely to have the same extent of necrosis in their central regions as the older 15 day old MTS. A comparison of average spectra revealed a slightly higher intensity at 1012 $cm^{-1}$ for the central region, consistent with observations in 15 day old MTS but most likely at the very initial stages of developing DNA damage associated with necrosis, making the distinction between regions must less clear than for 6 day old MTS. Comparing necrotic central regions of 6 and 15 day old MTS revealed a clear separation using PCA (Figure S3) again characterised predominantly by changes in the peaks at 963 $cm^{-1}$ and 1012 $cm^{-1}$.

Finally, to explore this intra-MTS change further, a region of the 15 day old untreated MTS was mapped with higher resolution (1 μm in the x and y directions) in order to investigate a cross sectional profile through the MTS. PCA was then used to identify the key spectral signatures that varied within the high resolution map of the 15 day old MTS (**Figure 7**). As expected, PC1 identified a general cellular Raman signal that distinguished cellular from non-cellular regions (Figure 7a-c). Interestingly, PC3 identified a component that had greatest abundance in the outer ring of the 15 day old MTS (Figure 7d-f), while PC4 identified a component that had greatest abundance in the inner necrotic core of the 15 day old MTS (Figure 7g-i). Upon investigating the loadings on PC3 and PC4, and representative spectra from regions with high abundance of PC3 and PC4, the outer region appeared to have a strong contribution from the peak at 963 $cm^{-1}$ (Figure 7e-f), while the inner region had a strong contribution from the peak at 1012 $cm^{-1}$ (Figure 7h-i). This is consistent with the previous hypothesis that the peak at 1012 $cm^{-1}$ was characteristic of a marker of necrosis as a result of DNA damage.

### 3.4. A new analytical tool for drug screening

This study has demonstrated the potential for Raman spectroscopy for analysis of MTS in a non-invasive and non-destructive manner, and has revealed some key changes in Raman spectral profile both as spheroids age and in response to drug treatment – primarily identifying changes in signals at 963 $cm^{-1}$ and 1012 $cm^{-1}$ to be responsive to ageing and drug treatment. For such an analytical tool to be useful for drug screening on MTS, a method for determining whether a particular drug induced a change in MTS biochemistry upon treatment is necessary. In the simplest manner, the intensity at particular key wavenumbers can be extracted for all points in each MTS dataset and compared. Figure 8 shows box and whisker plots for the distribution of values for both the 963 $cm^{-1}$ and 1012 $cm^{-1}$ intensities for MTS under each condition. Mann-Whitney tests were used to compare untreated and STS treated MTS for each intensity and revealed whether there was a statistically significant difference upon drug treatment. Therefore, this could be used as a statistically valid indicator as to whether to pursue a particular drug treatment further. Results are in line with previous observations, revealing both intensities to change in a statistically significant manner for 6 and 12 day old MTS and a statistically significant difference for the intensity at 1012 $cm^{-1}$ for 15 day old MTS but no significant difference for the intensity at 963 $cm^{-1}$. While there was a statistically significant difference for the intensity at 1012 $cm^{-1}$ for 15 day old MTS, the median value difference between untreated and treated MTS was low, a value that could act as a further indicator of the efficacy of a particular drug.

## 4. Conclusion

This study reports for the first time, Raman spectroscopic analysis of therapy response in multicellular tumour spheroids. While the 3D nature of MTS more closely mimics the *in vivo* tumour environment, analytical techniques for detailed and accurate analysis of MTS and spatially resolved changes in their biochemistry are limited. Here we explored the use of

Raman spectroscopy explored as a label free method to allow detailed molecular level analysis of MTS in attempt to reveal important biochemical changes in MTS as they age and in response to drug treatment. Principal component analysis combined with direct analysis of spectra revealed key spectral changes at 963 $cm^{-1}$ and 1012 $cm^{-1}$. Raman analysis could then be simplified to consider scatter plots of the intensity of these two peaks plotted against one another. The appearance of a peak at 1012 $cm^{-1}$ was probably indicative of DNA damage after induction of necrosis in 6 day old MTS treated with STS and as a result of necrotic core formation in 15 day old MTS. As the spheroids aged, the signal at 963 $cm^{-1}$ increased and we suggest that this is either due to the formation of microcalcifications or accumulated DNA damage. In addition, intra-MTS analysis of 15 day old MTS showed spatial variations in these spectral signals with the necrotic core region correlated strongly with the presence of a peak at 1012 $cm^{-1}$ and the outer regions containing more contribution from the 963 $cm^{-1}$ signal. Raman spectroscopy is therefore a powerful analytical tool for increasing understanding biochemical changes in ageing MTS (both inter- and intra-MTS) in addition to drug induced molecular changes in a label free manner with potential for high levels of spatial resolution. This information could be used to both reveal a more detailed understanding of spheroid biology, and provide Raman spectral markers to monitor in high throughput screening applications, potentially using statistical analysis to compare key peak intensities.

**Supporting Information**

Additional supporting information may be found in the online version of this article at the publisher's website.

Figure S1: Raman spectrum of paraffin

Figure S2: Comparison of central and outer regions of 6 day old MTS

Figure S3: Comparison of central regions of 6 and 15 day old MTS

## References


[1] C. Holohan, S. Van Schaeybroeck, D. B. Longley, P. G. Johnston *Nature Reviews Cancer*. **2013**, *13*, 714.
[2] N. Niu, L. Wang *Pharmacogenomics*. **2015**, *16*, 273-285.
[3] R.-Z. Lin, H.-Y. Chang *Biotechnology Journal*. **2008**, *3*, 1172-1184.
[4] L. E. Jamieson, D. J. Harrison, C. J. Campbell *Analyst*. **2015**, *140*, 3910-3920.
[5] G. Vlachogiannis, S. Hedayat, A. Vatsiou, Y. Jamin, J. Fernández-Mateos, K. Khan, A. Lampis, K. Eason, I. Huntingford, R. Burke, M. Rata, D.-M. Koh, N. Tunariu, D. Collins, S. Hulkki-Wilson, C. Ragulan, I. Spiteri, S. Y. Moorcraft, I. Chau, S. Rao, D. Watkins, N. Fotiadis, M. Bali, M. Darvish-Damavandi, H. Lote, Z. Eltahir, E. C. Smyth, R. Begum, P. A. Clarke, J. C. Hahne, M. Dowsett, J. de Bono, P. Workman, A. Sadanandam, M. Fassan, O. J. Sansom, S. Eccles, N. Starling, C. Braconi, A. Sottoriva, S. P. Robinson, D. Cunningham, N. Valeri *Science*. **2018**, *359*, 920.
[6] F. Hirschhaeuser, H. Menne, C. Dittfeld, J. West, W. Mueller-Klieser, L. A. Kunz-Schughart *Journal of Biotechnology*. **2010**, *148*, 3-15.
[7] K. M. Charoen, B. Fallica, Y. L. Colson, M. H. Zaman, M. W. Grinstaff *Biomaterials*. **2014**, *35*, 2264-2271.
[8] P. Worthington, D. J. Pochan, S. A. Langhans *Frontiers in Oncology*. **2015**, *5*, 92.
[9] C. R. Thoma, M. Zimmermann, I. Agarkova, J. M. Kelm, W. Krek *Advanced Drug Delivery Reviews*. **2014**, *69-70*, 29-41.
[10] D. Hanahan, Robert A. Weinberg *Cell*, *144*, 646-674.
[11] J. A. Nagy, S. H. Chang, A. M. Dvorak, H. F. Dvorak *British Journal of Cancer*. **2009**, *100*, 865-869.
[12] D. M. McDonald, P. Baluk *Cancer Research*. **2002**, *62*, 5381-5385.
[13] S. Däster, N. Amatruda, D. Calabrese, R. Ivanek, E. Turrini, R. A. Droeser, P. Zajac, C. Fimognari, G. C. Spagnoli, G. Iezzi, V. Mele, M. G. Muraro *Oncotarget*. **2017**, *8*, 1725-1736.
[14] L. E. Jamieson, V. L. Camus, P. O. Bagnaninchi, K. M. Fisher, G. D. Stewart, W. H. Nailon, D. B. McLaren, D. J. Harrison, C. J. Campbell *Nanoscale*. **2016**, *8*, 16710-16718.
[15] A. L. Harris *Nature Reviews Cancer*. **2002**, *2*, 38.
[16] M. Höckel, P. Vaupel *JNCI: Journal of the National Cancer Institute*. **2001**, *93*, 266-276.
[17] S. Azzi, J. K. Hebda, J. Gavard *Frontiers in Oncology*. **2013**, *3*, 211.
[18] Y.-C. Tung, A. Y. Hsiao, S. G. Allen, Y.-s. Torisawa, M. Ho, S. Takayama *Analyst*. **2011**, *136*, 473-478.
[19] M. Lee *American Journal of Pharmaceutical Education*. **2010**, *74*, 151.
[20] X. Gong, C. Lin, J. Cheng, J. Su, H. Zhao, T. Liu, X. Wen, P. Zhao *PLoS ONE*. **2015**, *10*, e0130348.
[21] J. Friedrich, C. Seidel, R. Ebner, L. A. Kunz-Schughart *Nature Protocols*. **2009**, *4*, 309.
[22] F. Pampaloni, N. Ansari, E. H. K. Stelzer *Cell and Tissue Research*. **2013**, *352*, 161-177.
[23] H. J. Butler, L. Ashton, B. Bird, G. Cinque, K. Curtis, J. Dorney, K. Esmonde-White, N. J. Fullwood, B. Gardner, P. L. Martin-Hirsch, M. J. Walsh, M. R. McAinsh, N. Stone, F. L. Martin *Nat. Protocols*. **2016**, *11*, 664-687.
[24] A. C. S. Talari, A. Raza, S. Rehman, I. U. Rehman *Applied Spectroscopy Reviews*. **2017**, *52*, 909-924.
[25] L. E. Jamieson, A. P. Bell, D. J. Harrison, C. J. Campbell in Monolayer to MTS: using SEM, HIM, TEM and SERS to compare morphology, nanosensor uptake and redox potential in MCF7 cells, Vol. 9531 (Ed.^Eds.: Editor), SPIE, City, **2015**, pp.10.

[26] V. L. Camus, G. Stewart, W. H. Nailon, D. B. McLaren, C. J. Campbell *Analyst*. **2016**, *141*, 5056-5061.
[27] S. Ōmura, Y. Asami, A. Crump *The Journal of Antibiotics*. **2018**, *71*, 688-701.
[28] L.-y. Xue, S.-m. Chiu, N. L. Oleinick *Experimental Cell Research*. **2003**, *283*, 135-145.
[29] L. Ruei-Zhen, C. Hwan-You *Biotechnology Journal*. **2008**, *3*, 1172-1184.
[30] K. J. M., T. N. E., B. C. J., F. Martin, N. L. K. *Biotechnology and Bioengineering*. **2003**, *83*, 173-180.
[31] J. Meehan, C. Ward, A. Turnbull, J. Bukowski-Wills, A. J. Finch, E. J. Jarman, C. Xintaropoulou, C. Martinez-Perez, M. Gray, M. Pearson, P. Mullen, C. T. Supuran, F. Carta, D. J. Harrison, I. H. Kunkler, S. P. Langdon *Oncotarget*. **2017**, *8*, 42857-42875.
[32] L. Jamieson, University of Edinburgh, **2016**.
[33] Z. Movasaghi, S. Rehman, I. U. Rehman *Applied Spectroscopy Reviews*. **2007**, *42*, 493-541.
[34] K. Czamara, K. Majzner, M. Z. Pacia, K. Kochan, A. Kaczor, M. Baranska *Journal of Raman Spectroscopy*. **2015**, *46*, 4-20.
[35] R. Herrmann, W. Fayad, S. Schwarz, M. Berndtsson, S. Linder *Journal of Biomolecular Screening*. **2008**, *13*, 1-8.
[36] E. W. Lipiec. **2013**.
[37] J. Ruiz-Chica, M. A. Medina, F. Sánchez-Jiménez, F. J. Ramírez *Biophysical Journal*. **2001**, *80*, 443-454.
[38] R. F. Cox, A. Hernandez-Santana, S. Ramdass, G. McMahon, J. H. Harmey, M. P. Morgan *British Journal Of Cancer*. **2012**, *106*, 525.

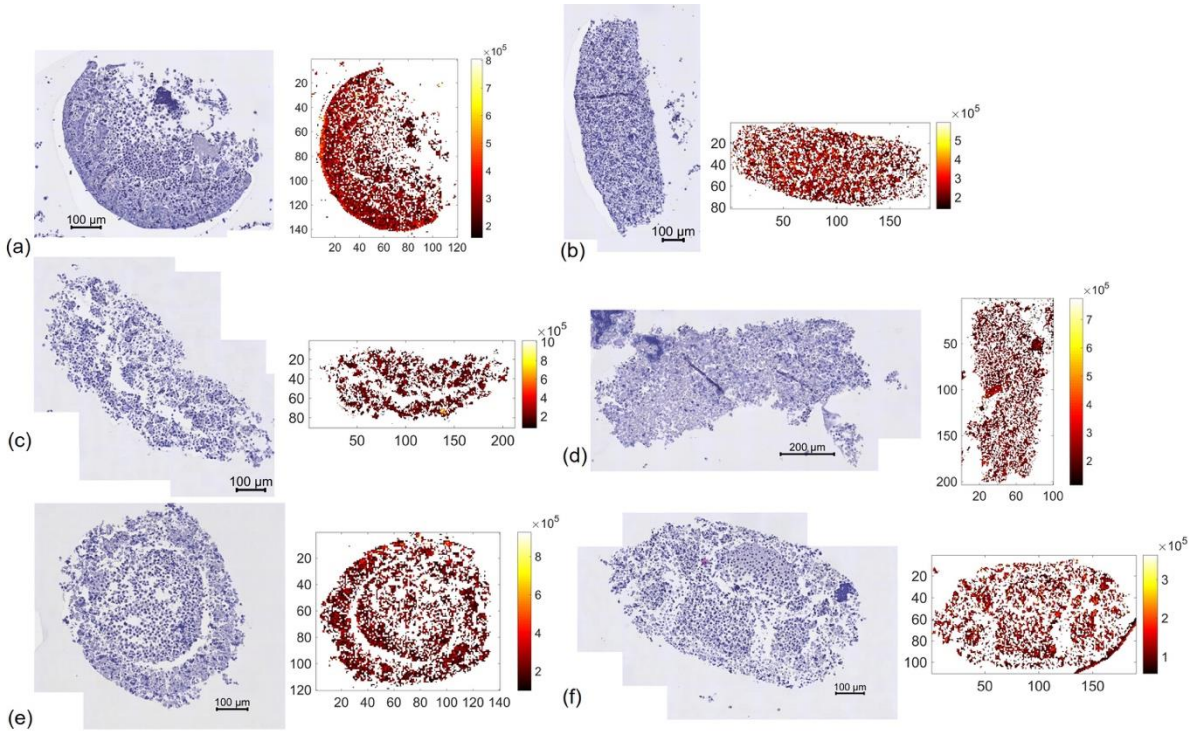


**Figure 1** Haematoxylin and Eosin stained multicellular tumour spheroids (left) and total Raman intensity of spheroid regions extracted for analysis from Raman maps (right) for untreated (a) and STS treated (b) 6 day old spheroids; untreated (c) and STS treated (d) 12 day old spheroids; and untreated (e) and STS treated (f) 15 day old spheroids. Spheroid sections were mapped on a Raman microscope using 5 µm steps in the x and y directions, 3 s

acquisition time, 50% laser power and a spectral centre of 1300 cm−1 and each unit in the x and y direction represents 5 µm.

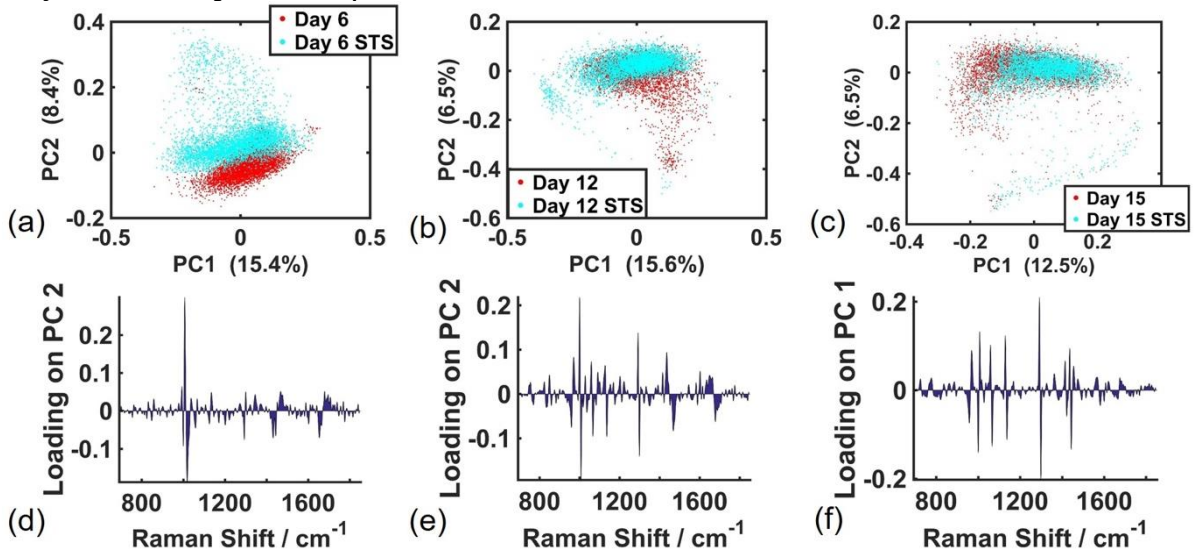


**Figure 2.** Principal component analysis was used to compare spectra from multicellular tumour spheroid sections mapped on a Raman microscope using 5 µm steps in the x and y directions, 3 s acquisition time, 50% laser power at 532 nm and a spectral centre of 1300 $cm^{-1}$. Spectra extracted from cell regions were compared for 6 day old spheroids with and without staurosporine (STS) treatment (a); 12 day spheroids with and without STS treatment (b); and 15 day old spheroids with and without STS treatment (c). The principal component loadings corresponding to the principal component (PC) over which conditions separated in each case – PC2 (d), PC2 (e) and PC1 (f) respectively – are given.

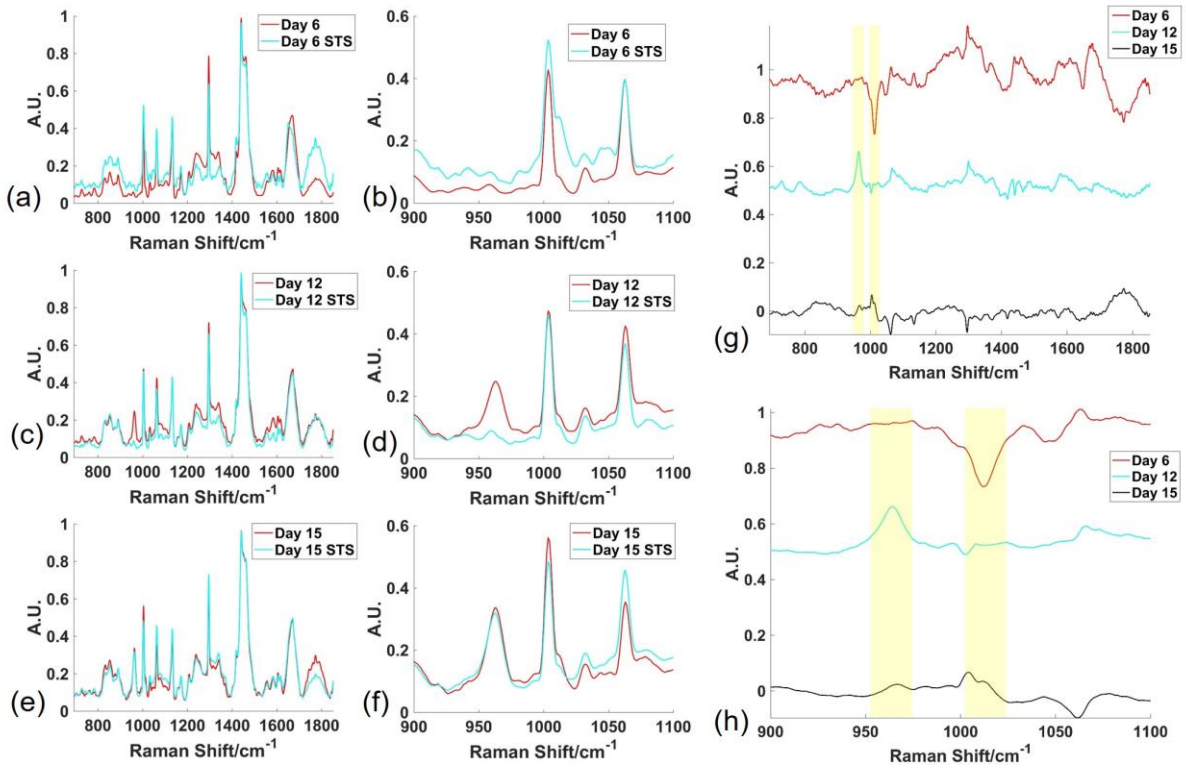


**Figure 3.** Average spectra from multicellular tumour spheroid sections mapped on a Raman microscope using 5 µm steps in the x and y directions, 3 s acquisition time, 50% laser power at 532 nm and a spectral centre of 1300 $cm^{-1}$. Spectra extracted from cell regions were compared for 6 day old spheroids with and without staurosporine (STS) treatment (a,b); 12 day spheroids with and without STS treatment (c,d); and 15 day old spheroids with and without STS treatment (e,f). Difference spectra of the mean STS treated condition subtracted from the mean untreated condition for each spheroid age are given (g,h) to emphasise the regions of maximal change. Difference spectra are offset by 0.5 for clarity and peaks at 963 $cm^{-1}$ and 1012 $cm^{-1}$ are highlighted in yellow.

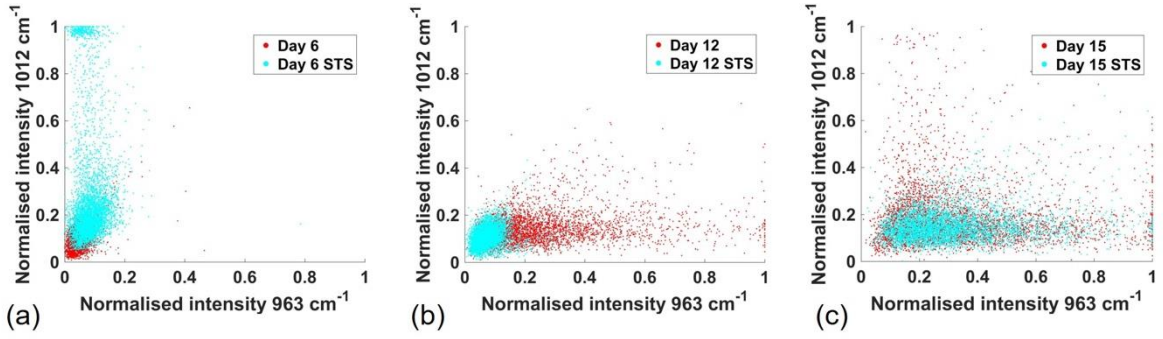


**Figure 4.** Scatter plots of the intensity of the peak at 1012 $cm^{-1}$ and intensity of the peak at 963 $cm^{-1}$ from spectra from multicellular tumour spheroid sections mapped on a Raman microscope using 5 µm steps in the x and y directions, 3 s acquisition time, 50% laser power at 532 nm and a spectral centre of 1300 $cm^{-1}$. Plots are compared for 6 day old spheroids with and without staurosporine (STS) treatment (a); 12 day spheroids with and without STS treatment (b); and 15 day old spheroids with and without STS treatment (c).

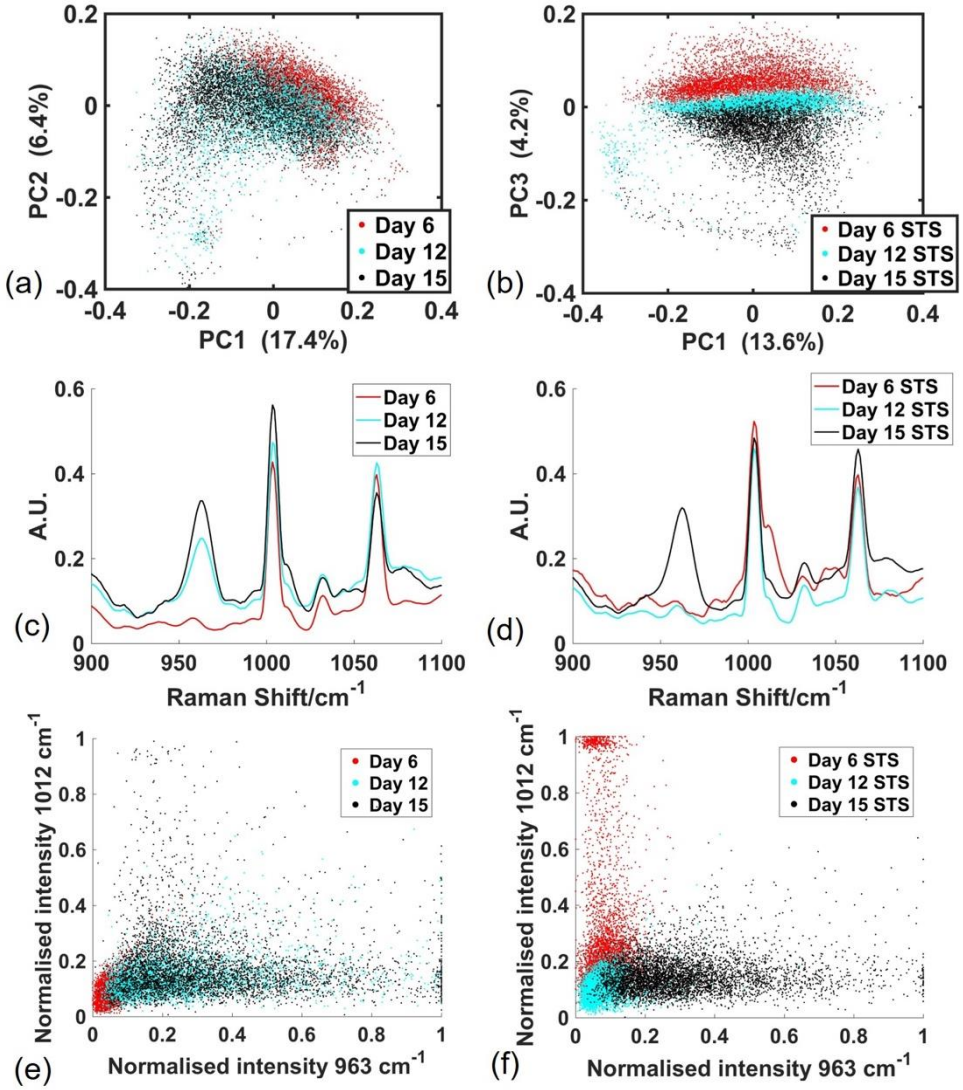


**Figure 5.** Principal component analysis (PCA) was used to compare spectra from multicellular tumour spheroid sections mapped on a Raman microscope using 5 µm steps in the x and y directions, 3 s acquisition time, 50% laser power at 532 nm and a spectral centre of 1300 $cm^{-1}$. Spectra extracted from cell regions were compared using PCA for untreated 6, 12 and 15 day old spheroids (a); and for STS treated 6, 12 and 15 day old spheroids (b). Average spectra for untreated (c) and STS treated (d) 6, 12 and 15 day old spheroids; and scatter plots of the intensity of the peak at 1012 $cm^{-1}$ and intensity of the peak at 963 $cm^{-1}$ for untreated (e) and STS treated (f) 6, 12 and 15 day old spheroids are also compared.

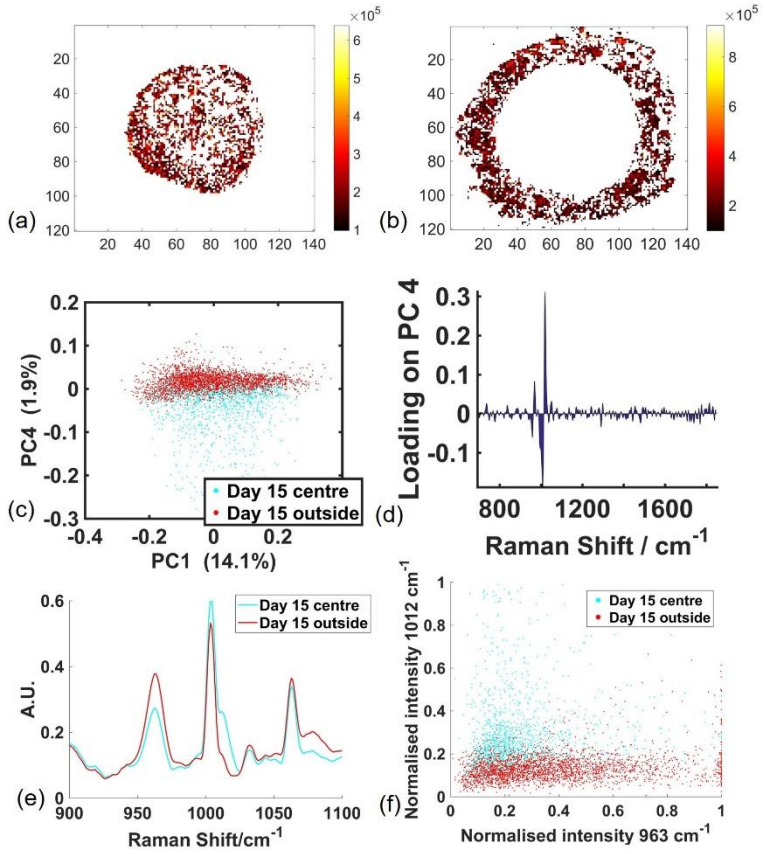


**Figure 6.** Extracted Raman spectra from a 15 day old multicellular tumour spheroid section mapped on a Raman microscope using 5 μm steps in the x and y directions, 3 s acquisition time, 50% laser power at 532 nm and a spectral centre of 1300 $cm^{-1}$ were separated into central (a) and outer (b) regions (colour scale corresponds to total spectral intensity and spatial coordinates to μm). Spectra extracted from central and outer regions were compared using PCA (c), where they separated on principal component 4 (d). Average spectra of the regions compared (e) and scatter plots of the intensity of the peak at 1012 $cm^{-1}$ and intensity of the peak at 963 $cm^{-1}$ (f) are also compared.

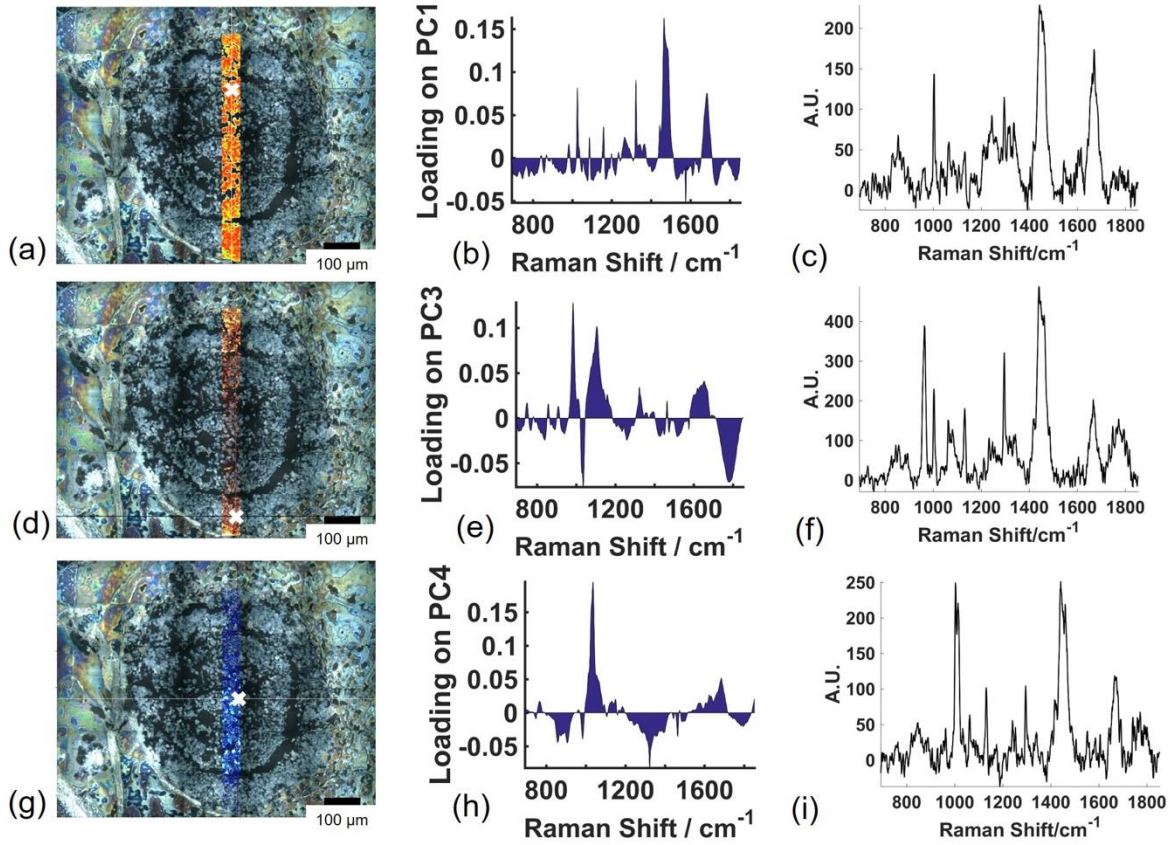


**Figure 7.** A high resolution cross section through a 15 day old multicellular tumour spheroid was mapped on a Raman microscope using 1 µm steps in the x and y directions, 1 s acquisition time, 50% laser power at 532 nm and a spectral centre of 1300 $cm^{-1}$. Principal component analysis (PCA) on this map revealed principal component (PC) 1 to correlate with cell regions (a), where the loadings on PC1 (b) correlated with common cell Raman signals and a representative example spectrum from the point indicated with the white cross in (a) is given (c). PC3 showed higher intensity in the outer regions of the spheroid (d), where the loadings on PC3 (e) had primary contribution from the signal and 963 $cm^{-1}$ and a representative example spectrum of high intensity from the point indicated with the white cross in (d) is given (f). PC4 showed higher intensity in the central regions of the spheroid (g), where the loadings on PC4 (h) had primary contribution from the signal and 1012 $cm^{-1}$ and a representative example spectrum of high intensity from the point indicated with the white cross in (g) is given (i).

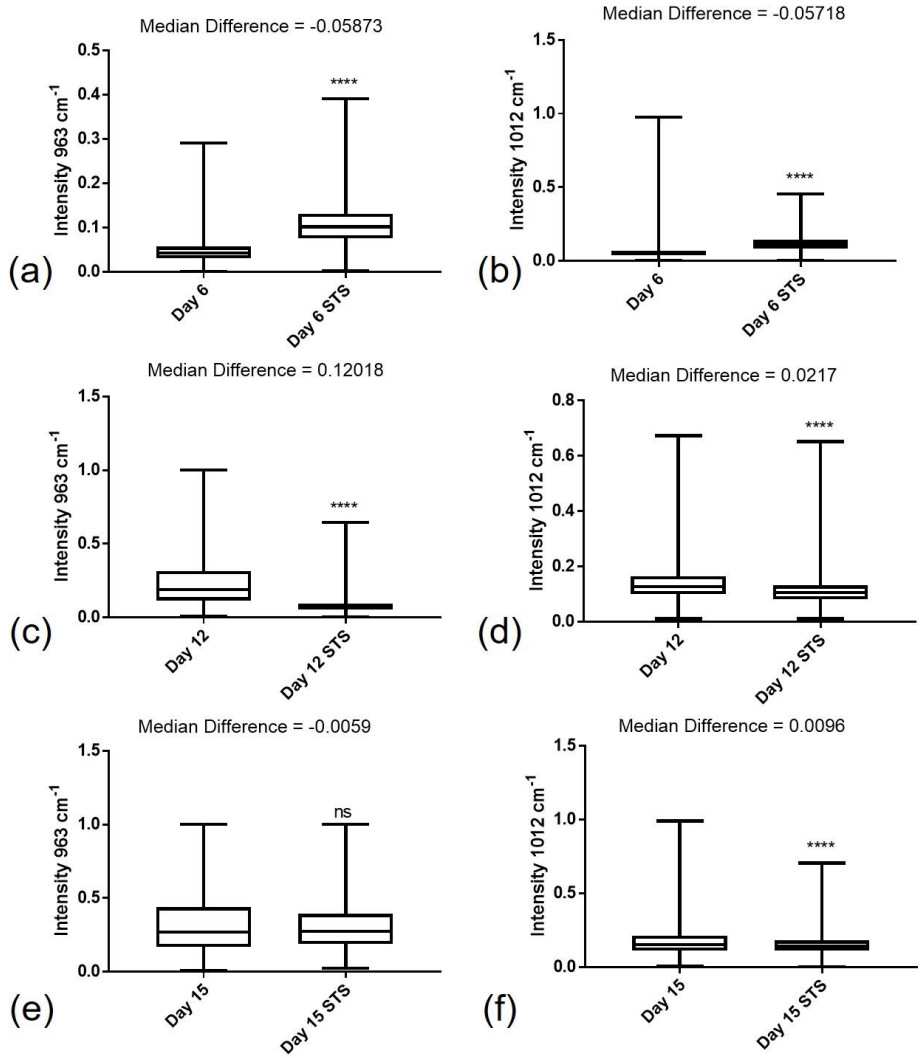


**Figure 8.** Box and whiskers plots (minimum, 1st quartile, median, 3rd quartile, maximum) of the distribution of intensities at 963 $cm^{-1}$ (a,c,e) and 1012 $cm^{-1}$ (a,c,e) for 6 (a,b), 12 (c,d) and 15 (e,f) day old MTS both untreated and treated with treated with STS. The difference between the untreated and STS treated median values is given in each case and Mann-Whitney tests were performed in each case: **** = $p<0.0001$; ns = not significant.